

Supporting Information (SI)

for

Nitrogen-doped carbon nanotubes encapsulating Fe/Zn nanoparticles as persulfate activator for sulfamethoxazole degradation: role of encapsulated bimetallic nanoparticles and nonradical reaction

Shang Yanan^a, Xu Xing^a, Qinyan Yue^{*,a}, Baoyu Gao^{*,a}, Yanwei Li^b

^a Shandong Key Laboratory of Water Pollution Control and Resource Reuse, School of Environmental Science and Engineering, Shandong University, No. 72 Binhai Road, Jimo District, Qingdao City 266237, Shandong province, P.R. China.

^b Environmental Research Institute, Shandong University, No. 72 Binhai Road, Jimo District, Qingdao City 266237, Shandong province, P.R. China.

Appendix S1

Electron paramagnetic resonance (EPR) and reactive oxygen species (ROS) capture test:

The occurrence of radical species such as $\text{SO}_4^{\cdot-}$ and $\cdot\text{OH}$ was examined with an electron paramagnetic resonance (EPR) spectroscopy (A300, Bruker Co.) using 10 mM 5,5-dimethyl-1-pyrroline N-oxide (DMPO) as a spin-trapping agent. TMP was used to mark $^1\text{O}_2$ which would oxidize TMP into 2,2,6,6-tetramethyl-4-piperidinol-N-oxyl radical (TMPN). The sample was placed in a quartz flat cell and analyzed under the following conditions: microwave frequency = 9.64 GHz, microwave power = 0.94mW, modulation frequency = 100 kHz, and modulation amplitude = 2.0 G.

*Corresponding author: Tel.: +86-531-88361912; Fax: +86-531-88364513
E-mail: qyyue58@aliyun.com

*Corresponding author: Tel.: +86-531-88361912; Fax: +86-531-88364513
E-mail: baoyugao_sdu@aliyun.com

Appendix S2

Characterization Analysis Section:

The morphology of catalyst was characterized via a high resolution transmission electron microscopy (FEI Tecnai G2 F20 S-TWIN) at 200 kV and a field-emission scanning electron microscope (FE-SEM, Hitachi, SU8010) at 5 kV. The X-ray diffraction (XRD) patterns were obtained to analysis the crystal structure of the samples on a X'Pert PRO MPD X-ray instrument using Cu-K α radiation ($\lambda=0.15406$ nm) with at a scanning rate of 10° per minute. The surface chemical compositions and states of the catalysts were measured by Raman spectra (LabRam-1B French Dilor Com, $\lambda_{ex} = 532$ nm), and X-ray photoelectron spectroscopy (XPS, Thermo Escalab 250, Al-K α X-rays). Zeta potential of the aqueous-suspended samples were measured using Zetasizer Nano ZS (Malvern). An inductive coupled plasma (ICP) emission spectrometer (PerkinElmer 8300) was used to determine concentration of metal ion in solution. LC-MS (Thermo, LCQ FLEET) operating in a positive mode. The scan range was from 100 m/z (mass to charge ratio) to 500 m/z.

Appendix S3

Theoretical calculations:

The Fukui functions and were performed at the B3LYP/6-31G(d) level using the Gaussian 09 program. The structural geometry optimization was used to confirm a true energy minimum on the potential energy surface. The models of carbon nanotubes (CNTs) and various nitrogen doped (pyridinic N, pyrrolic N, and graphitic N) CNTs were constructed via TubeGen 3.4[1] and GaussView 5.0. The dangling bonds of the tip atoms of the CNTs were terminated with H atoms to obtain a neutral cluster. All calculations were performed with the Gaussian 09 program. The B3LYP/6-31G(d) method was used to optimize the models where the water was set for the solvation effect. The ESP distributions were constructed with GaussView 5.0 on the basis of the B3LYP/6-31G(d)-optimized results. Due to the size and edge effects, the properties estimated with the finite-size model may vary from those of the real system to some extent. However, it can be expected that the results obtained with the current model would be qualitatively reliable in predicting the local chemical

properties[2].

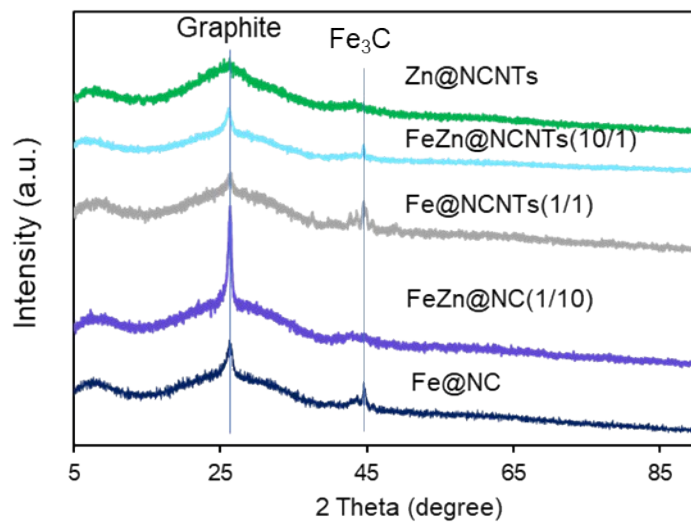


Figure S1. XRD patterns of the Fe@NC, Zn@NC and various FeZn@NC.

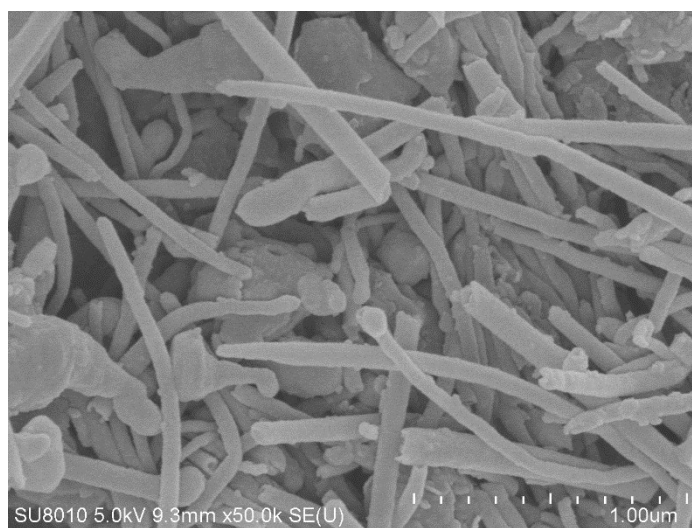


Figure S2. SEM image of FeZn@NC(1/10).

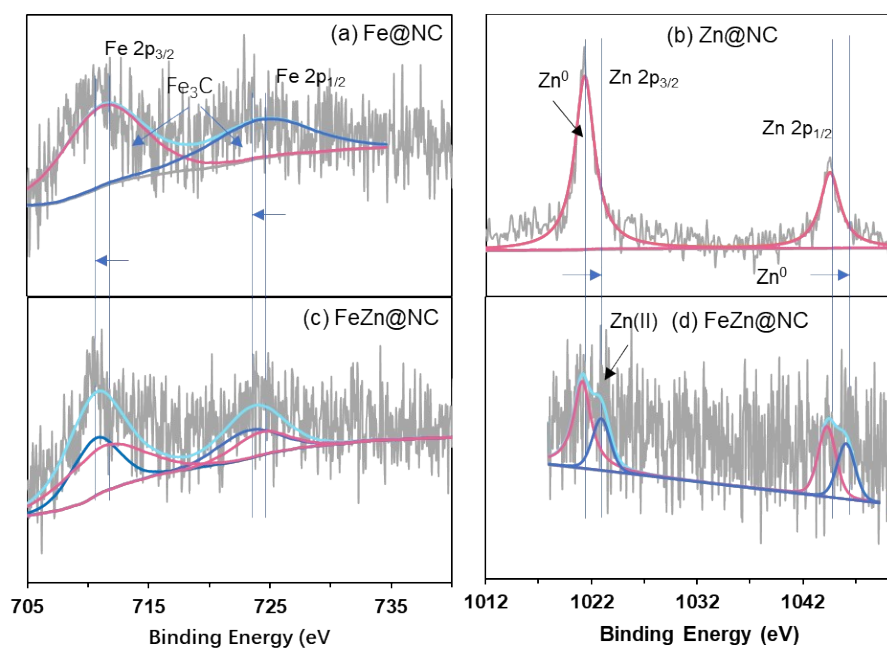


Figure S3. Fe 2p XPS spectra of (a) Fe@NC and (c) FeZn@NC, Zn 2p XPS spectra of (b) Zn@NC and (d) FeZn@NC.

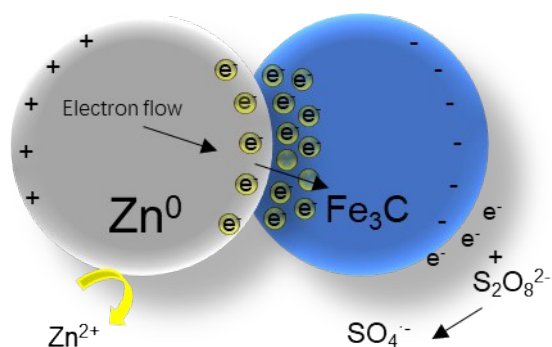


Figure S4. The proposed interaction between bimetal species.

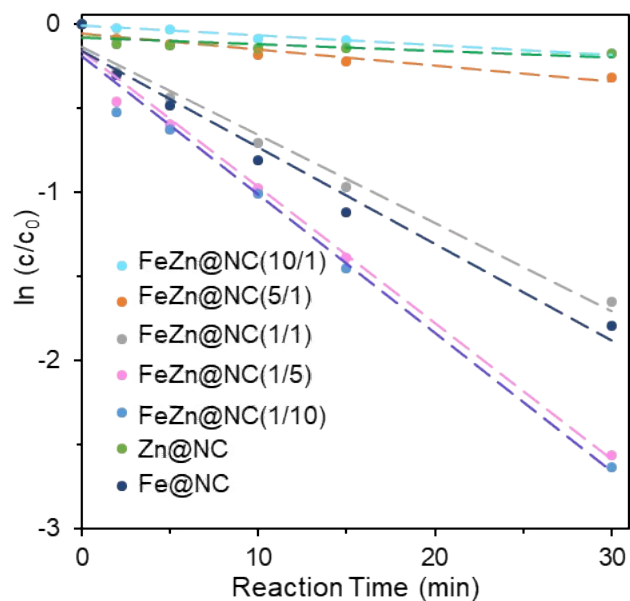


Figure S5. Pseudo-first-order kinetic models for SMX degradation by various FeZn@NC, Zn@NC and Fe@NC ($[PS]_0=1$ mM, $[SMX]_0=5$ mg/L, catalyst dosage= 0.1 g L $^{-1}$).

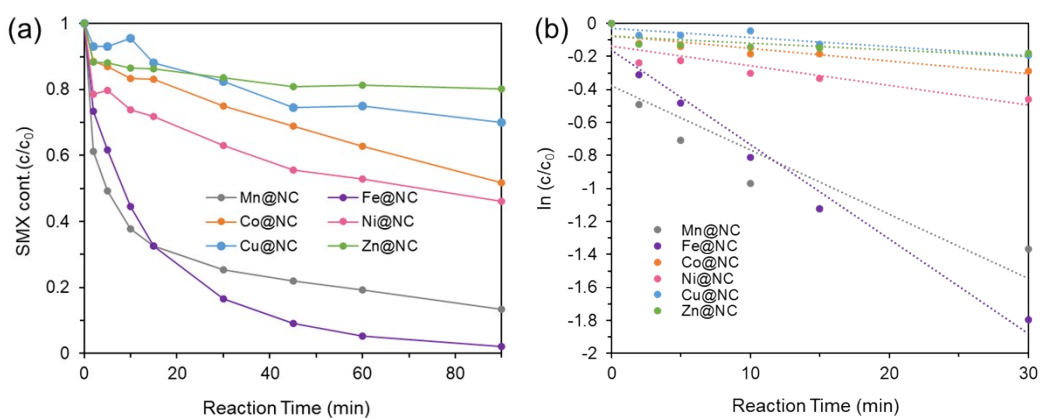


Figure S6. SMX degradation by Mn@NC, Fe@NC, Co@NC, Ni@NC, Cu@NC and Zn@NC. (a) degradation kinetics curves; (b) Pseudo-first-order kinetic models ($[PS]_0=1$ mM, $[SMX]_0=5$ mg/L, catalyst dosage= 0.1 g L $^{-1}$).

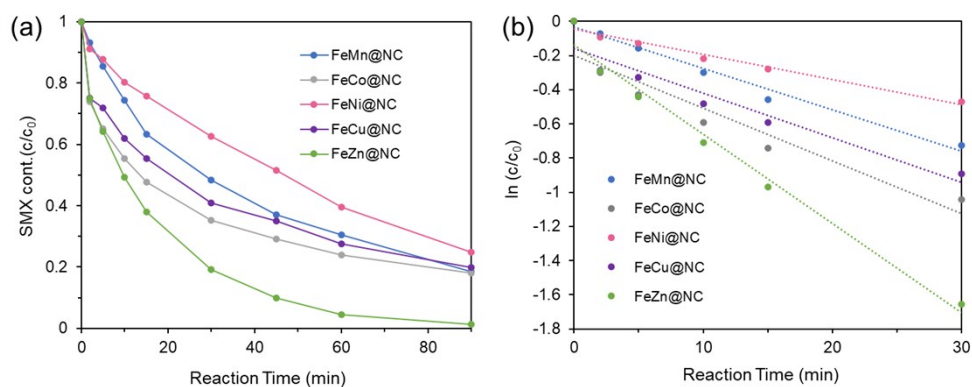


Figure S7. SMX degradation by FeMn@NC, FeCo@NC, FeNi@NC, FeCu@NC and FeZn@NC. (a) degradation kinetics curves; (b) Pseudo-first-order kinetic models ($[PS]_0=1$ mM, $[SMX]_0=5$ mg/L, catalyst dosage= 0.1 g L⁻¹).

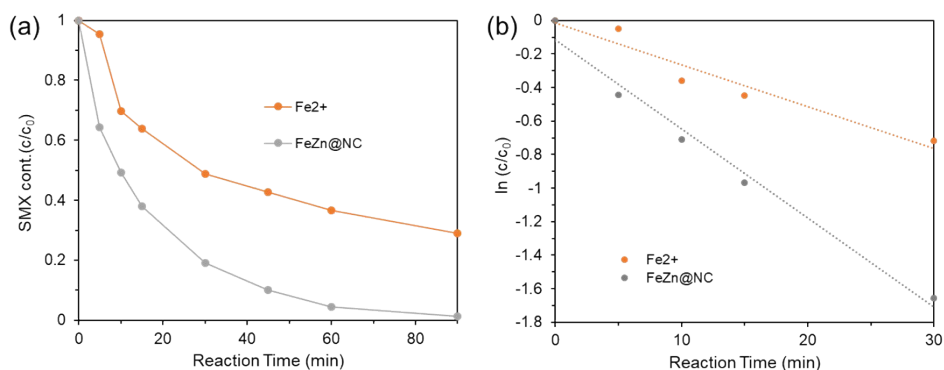


Figure S8. SMX degradation by Fe²⁺ and FeZn@NC. (a) degradation kinetics curves; (b) Pseudo-first-order kinetic models ($[PS]_0=1$ mM, $[SMX]_0=5$ mg/L, catalyst dosage= 0.1 g L⁻¹).

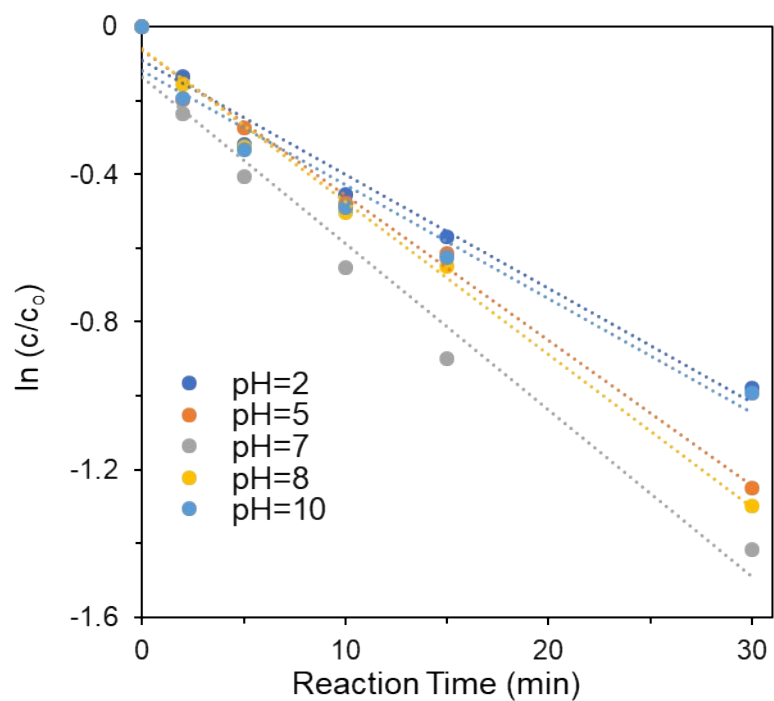


Figure S9. Pseudo-first-order kinetic models for SMX degradation by FeZn@NC in various pH. ($[PS]_0=1$ mM, $[SMX]_0=5$ mg/L, catalyst dosage= 0.1 g L $^{-1}$).

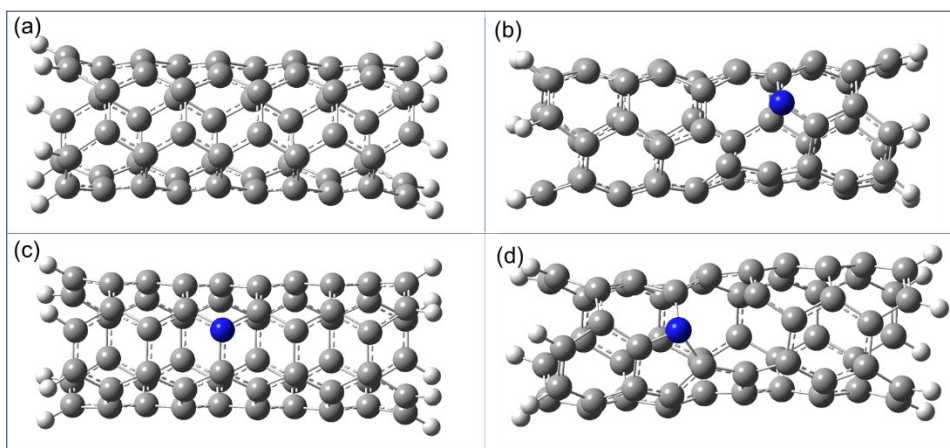


Figure S10. Simulated structure of (a) pristine carbon nanotube, (b) pyridinic N doped carbon nanotube, (c) graphitic N doped carbon nanotube and (d) pyrrolic N doped carbon nanotube.

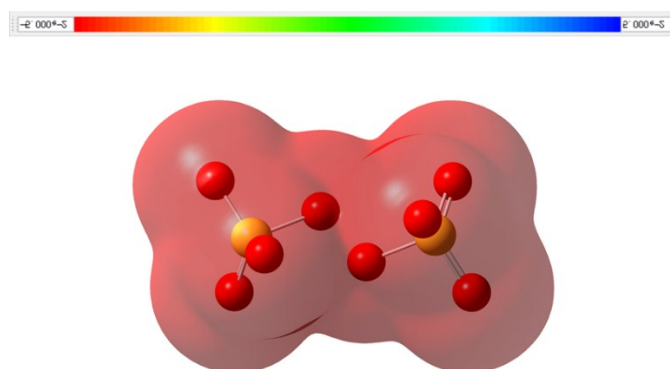
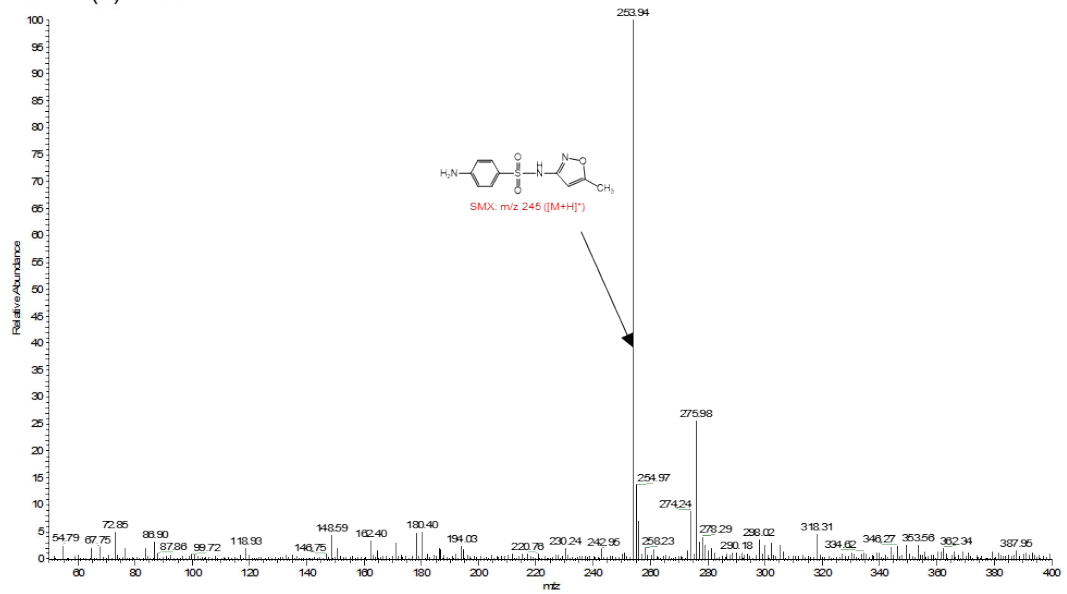
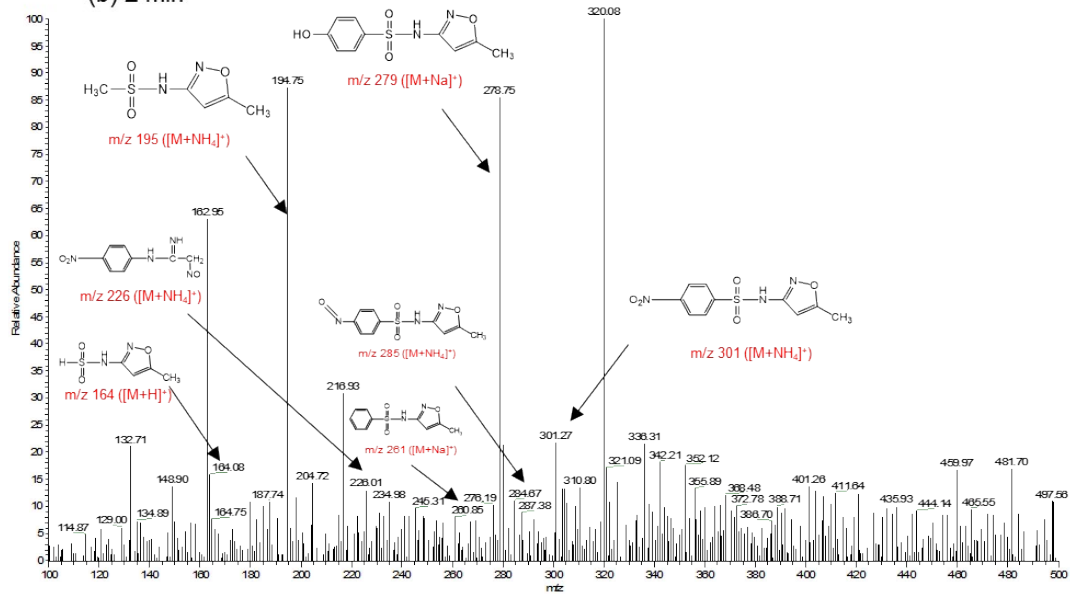


Figure S11. ESP of the persulfate molecule.

(a) 0 min



(b) 2 min



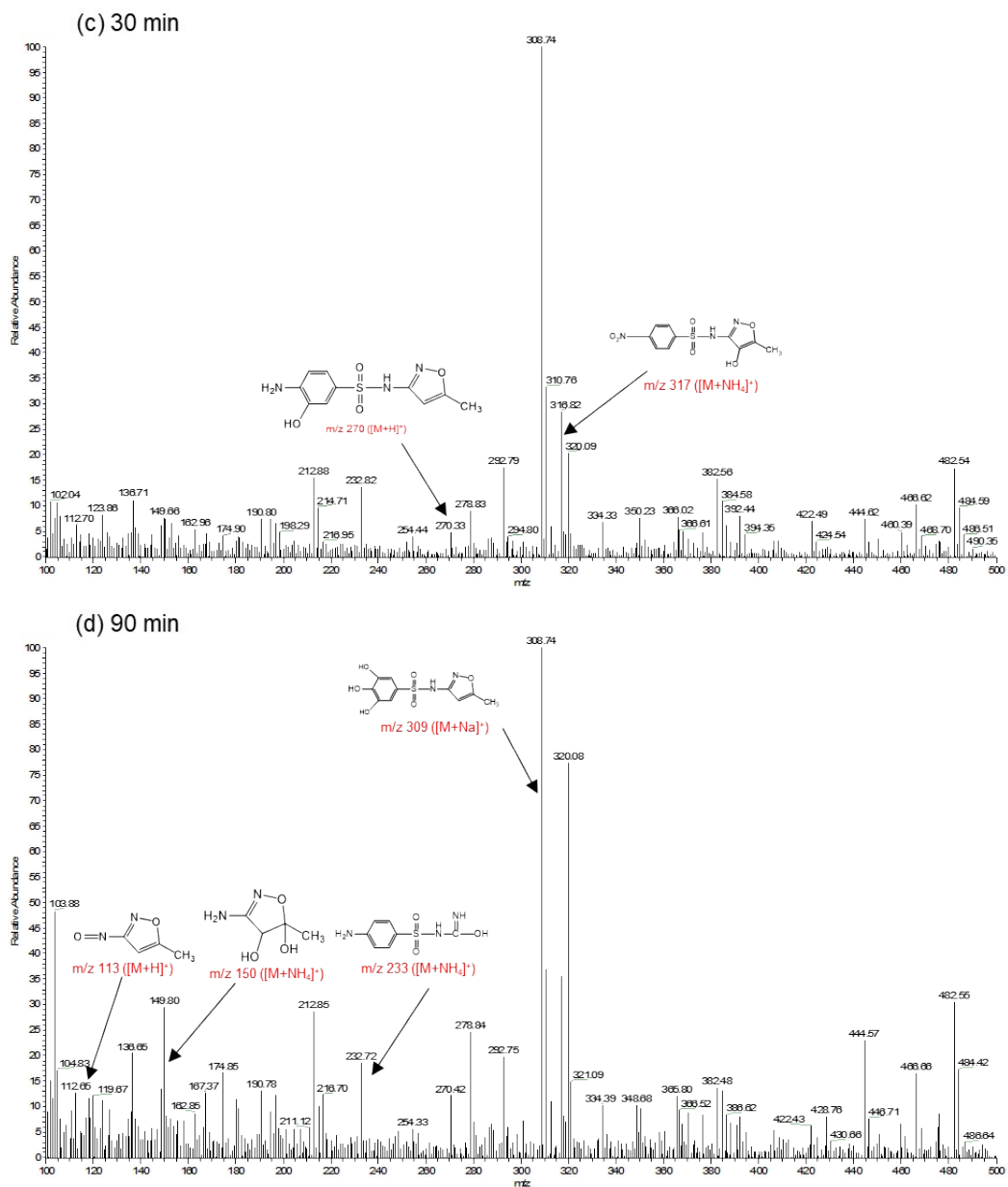


Figure S12. LC-MS spectra of the intermediates of SMX in the FeZn@NC PS system at different time intervals: (a) 0 min, (b) 2 min, (c) 5min, (d) 30 min, (e) 90 min.

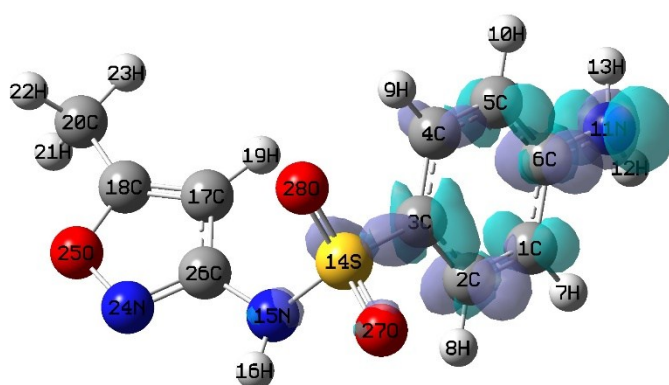


Figure S13. Isosurface map of the dual descriptor. The isovalue is 0.004. Purple and green surfaces correspond to positive and negative regions, respectively.

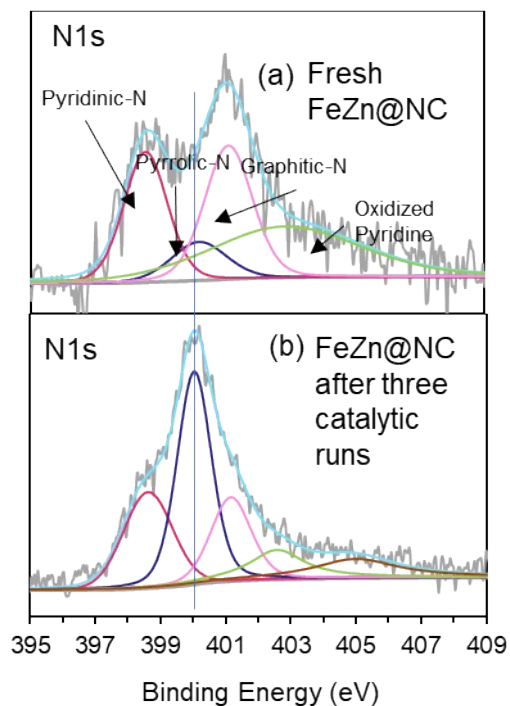


Figure S14. Comparison of high resolution XPS spectra of (a) fresh FeZn@NC and (b) FeZn@NC after three catalytic runs.

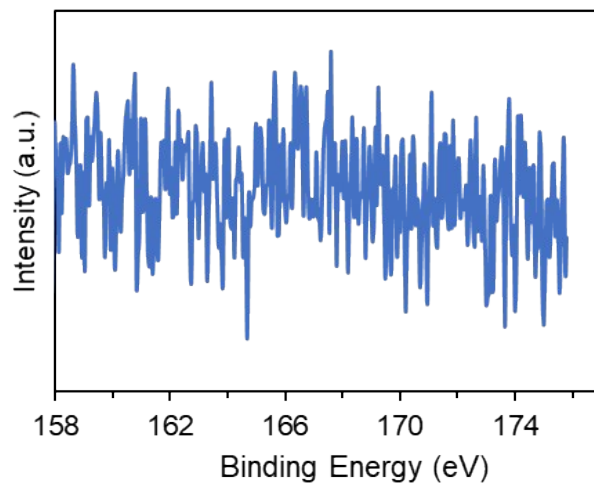


Figure S15. High resolution XPS spectra of the S region of the FeZn@NC.

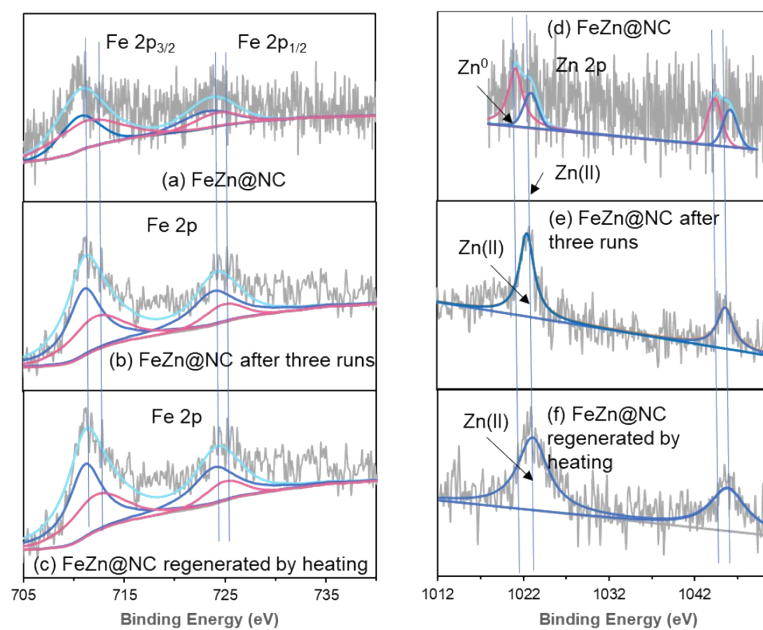


Figure S16. High-resolution Fe2p (a-c) and Zn2p (d-f) XPS spectrum of FeZn@NC, FeZn@NC after three runs and FeZn@NC regenerated by heating.

Table S1 the amount of raw material of serial ZnFe@NC

Denomination	Amount of raw materials		
	ZnCl ₂	FeCl ₃ ·6H ₂ O	Melamine
Fe@NC	-	19.88 g	10.00 g
FeZn@NC(10/1)	18.00 g	1.00 g	10.00 g
FeZn@NC(5/1)	16.67 g	1.67 g	10.00 g
FeZn@NC(1/1)	10.02 g	19.88 g	10.00 g
FeZn@NC(1/5)	8.33 g	3.33 g	10.00 g
FeZn@NC(1/10)	9.09 g	1.81 g	10.00 g
Zn@NC	10.02 g	-	10.00 g

Table S2 the adsorption energies (ΔE_{ads}) between PS and various N doped NCNTs

Type of carbon nanotubes	ΔE_{ads} (eV)
pristine CNTs	-0.194
pyridinic N	-0.910
graphitic N	-0.025
pyrrolic N	-0.295

References

- [1] J. T. Frey and D. J. Doren, Newark DE, TubeGen 3.4, web-interface, <http://turin.nss.udel.edu/research/tubegenonline.html>, (2011).
- [2] L. Lyu, G. Yu, L. Zhang, C. Hu, Y. Sun, 4-Phenoxyphenol-Functionalized Reduced Graphene Oxide Nanosheets: A Metal-Free Fenton-Like Catalyst for Pollutant Destruction, *Environmental science & technology*, 52 (2017) 747-756.